Supporting Information

Nanooptical designs enhance monolithic Perovskite/Silicon Tandem Solar Cells toward 29.8% Efficiency

Philipp Tockhorn[1#], Johannes Sutter[1#], Alexandros Cruz[1], Philipp Wagner[1], Klaus Jäger[1,2], Danbi Yoo[1], Felix Lang[3], Max Grischek[1,3], Bor Li[1], Amran Al-Ashouri[1], Eike Köhnen[1], Martin Stolterfoht[3], Dieter Neher[3], Rutger Schlatmann[1,5], Bernd Rech[1,4], Bernd Stannowski[1], Steve Albrecht[1,4], Christiane Becker[1,5]**

[1] Helmholtz-Zentrum Berlin für Materialien und Energie GmbH, Division Solar Energy, Kekuléstr. 5, 12489, Berlin, Germany

[2] Zuse Institute Berlin, Computational Nanooptics Group, Takustr. 7, 14195 Berlin, Germany

[3] Universität Potsdam, Soft matter physics, Karl-Liebknecht-Straße 24/25, 14476 Potsdam, Germany

[4]Technische Universität Berlin, Faculty of Electrical Engineering and Computer Science, 10587 Berlin, Germany

[5]Hochschule für Technik und Wirtschaft Berlin, Faculty 1: School of Engineering – Energy and Information, 10313 Berlin, Germany

# These authors contributed equally to this work. Order determined by cast of 298 sided digital dice.

* Email: steve.albrecht@helmholtz-berlin.de, christiane.becker@helmholtz-berlin.de

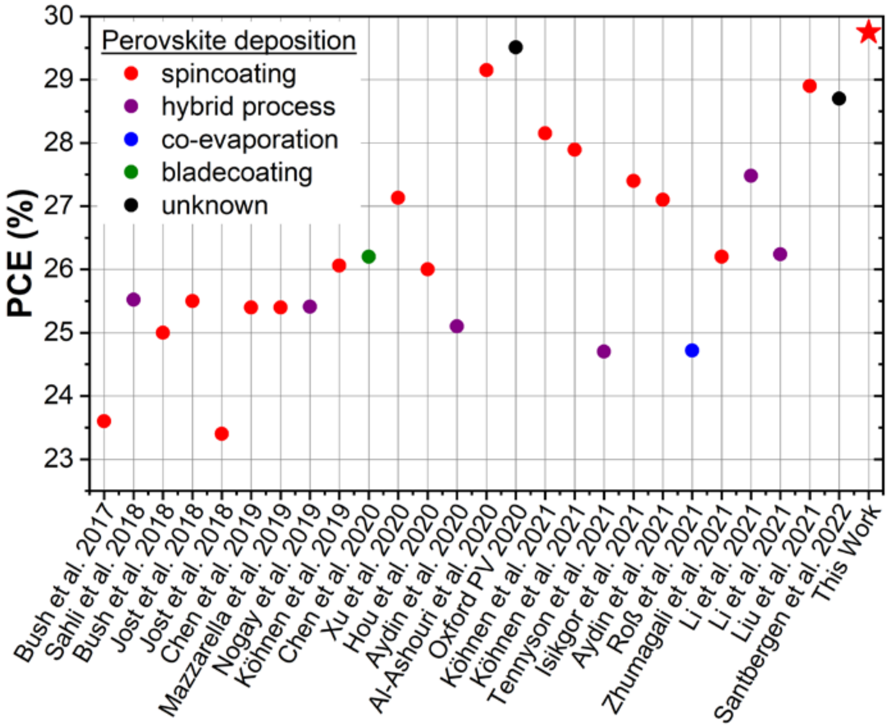

Figure S1 | Overview of 2-terminal perovskite/silicon tandem solar cells (PSTSC) with power conversion efficiency (PCE) >23%. The different colors mark the deposition technique of the perovskite absorber, as displayed in the legend.

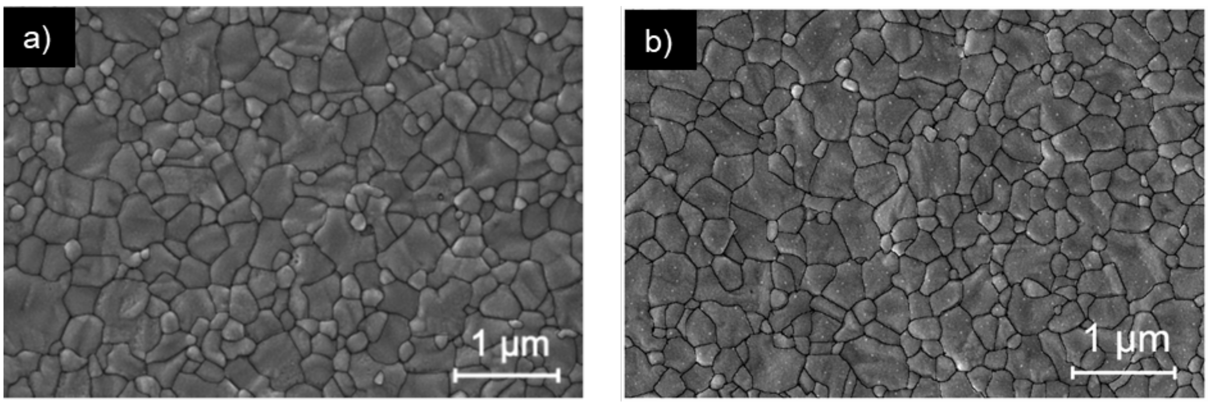

Figure S2 | Top-view scanning electron microscope (SEM) images of perovskite layers deposited on planar (a) and nanotextured (b) substrates. The grain size analysis in Fig. 2c is based on these images.

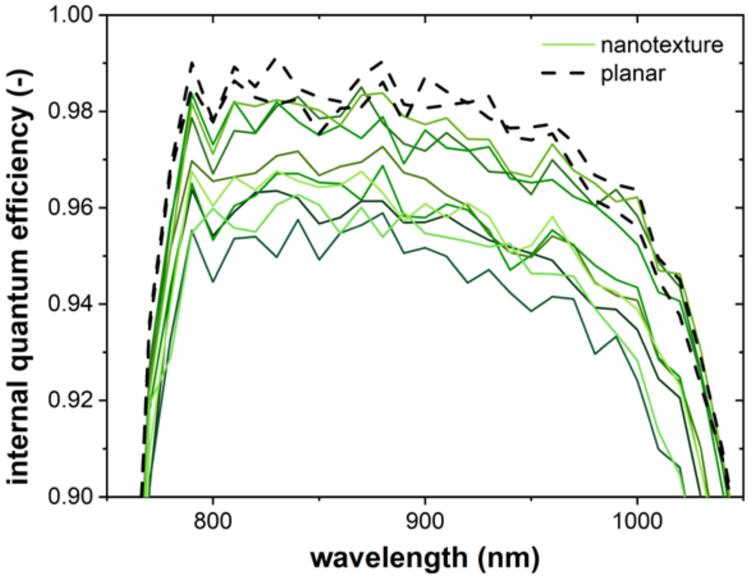

Figure S3 | Internal quantum efficiency (IQE) defined as IQE = EQE/(1-*R*) of planar (black dashed lines) and nanotextured silicon bottom cells (green lines).

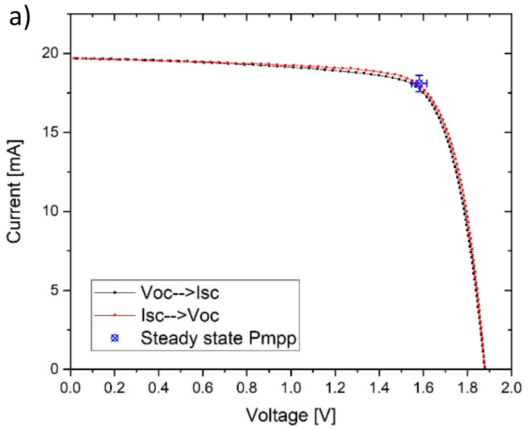

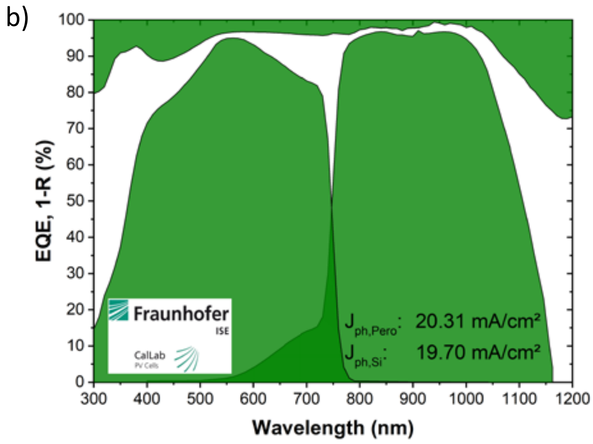

Figure S4 | (a) Current/voltage (*J*-*V*) characteristics of a nanotextured PSTSC with standard rear reflector (no RDBL) certified by CalLab at Fraunhofer ISE. The maximum power point (MPP) value is marked as a blue cross. (b) Corresponding external quantum efficiency (EQE) measurement of a nanotextured PSTSC with standard rear reflector with summed up short circuit current density from EQE ($J_{ph,pero}$+$J_{ph,Si}$) = 40 mA/cm^2 the 1-*R* spectrum was measured in-house. Note that the EQE spectra were measured in the wavelength range from 300-1162 nm, which leads to a slight underestimation of the photogenerated current density of the silicon subcell.

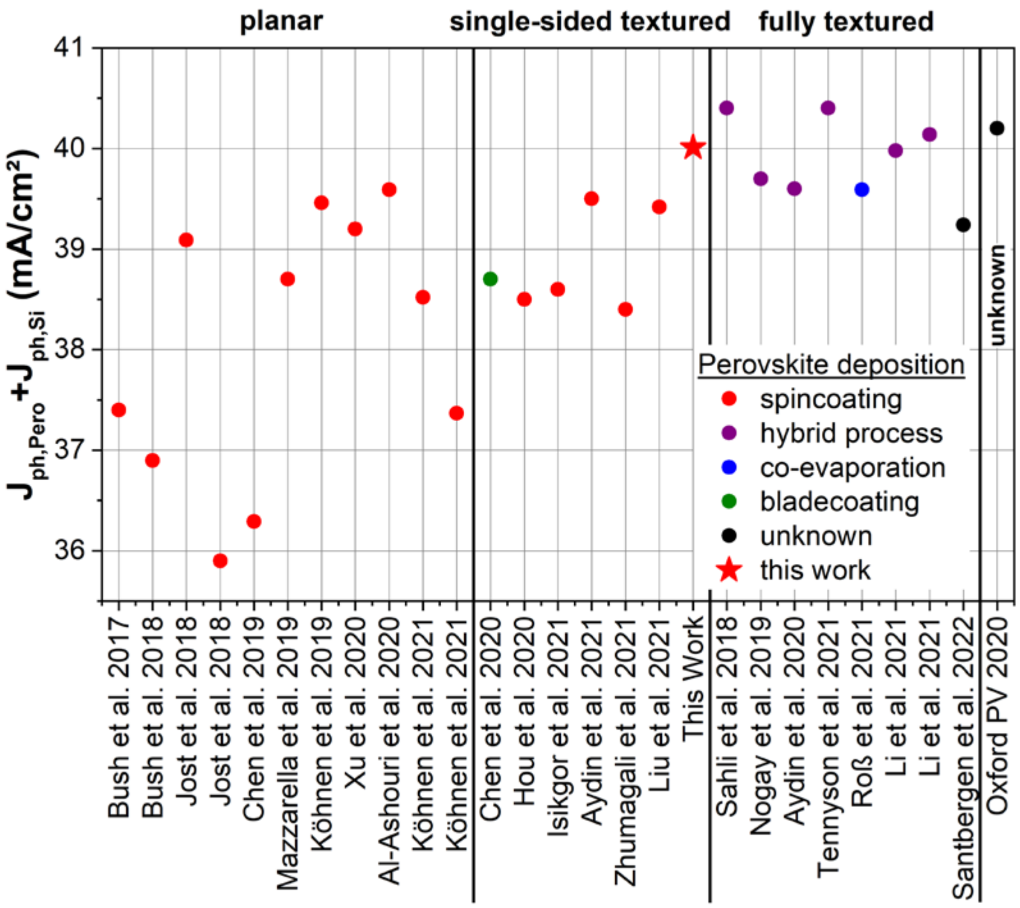

Figure S5: Combined photogenerated current density of perovskite and silicon sub cell ($J_{ph,Pero}$+$J_{ph,Si}$) for selected publications of highly efficient perovskite/silicon tandem solar cells (PSTSC). The values are taken from the reported EQE-spectra in the respective publications. The graph is structured into PSTSCs with planar, single-sided and fully textured perovskite top cell.

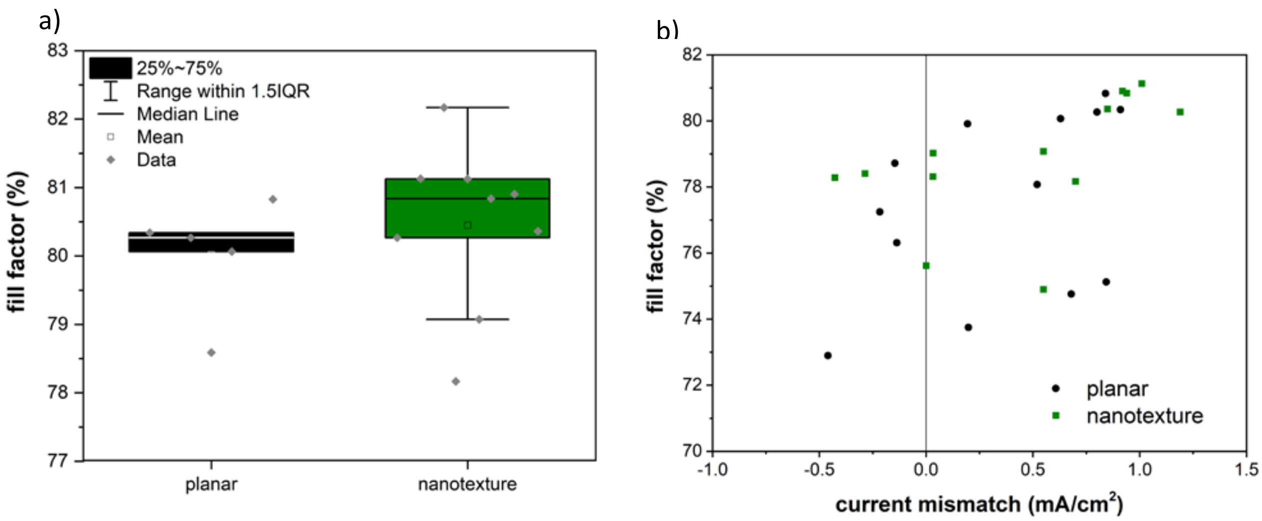

Figure S6 | (a) Boxplots of the fill factor for nanotextured and planar tandem solar cells (one batch). (b) Fill factor *(FF)* of various planar and nanotextured perovskite/silicon tandem solar cells (PSTSC) as a function of current mismatch ($J_{ph,Pero}$ - $J_{ph,Si}$) (various batches with bandgaps of 1.66 eV - 1.68 eV).

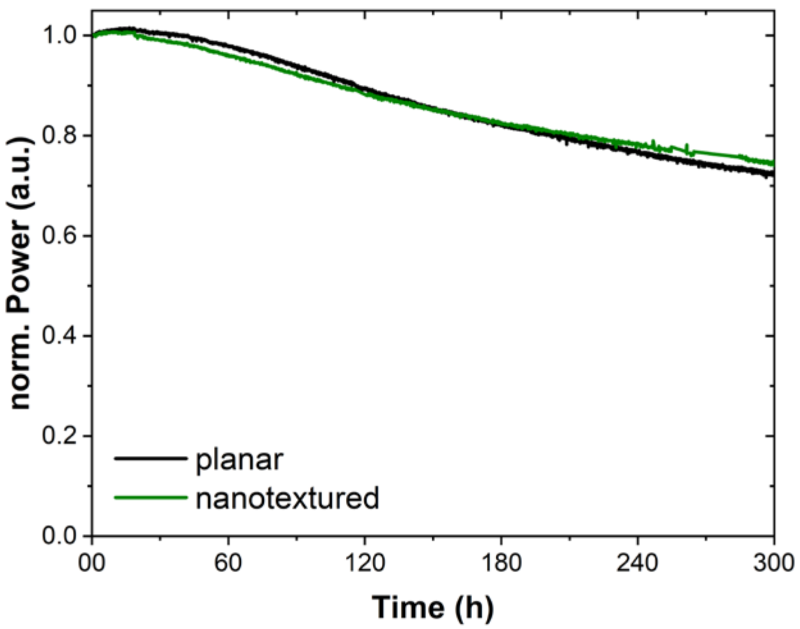

Figure S7 | Long-term maximum power point (MPP) track under a dichromatic LED illumination of non-encapsulated perovskite/silicon tandem solar cells (PSTSC) in air at a controlled temperature of 25°C and relative humidity of 30 to 40%.

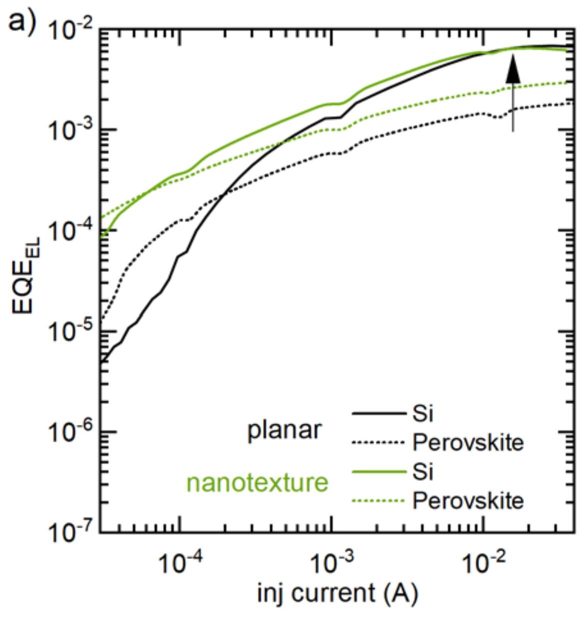

Figure S8 | Electroluminescence quantum yield (EQE_{EL}) of the perovskite and c-Si subcells in planar and nanotextured perovskite/silicon tandem solar cells (PSTSC). Interestingly, the Si EQE_{EL} changes barely, while the Perovskite increases by approximately 60% (relative) for the nanotextured device compared to the planar PSTSC.

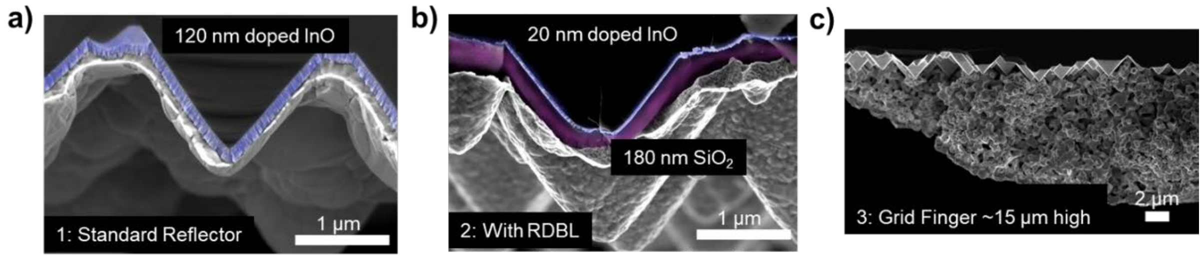

Figure S9 | Cross-sectional scanning electron microscopy (SEM) images of different rear reflectors: 1. Standard reflector, 2. reflector with dielectric buffer layer (RDBL) and 3. Local contacts of the RDBL.

Figure S10 | Certificate of the 29.8% efficient PSTSC

1. Beschreibung des Messgegenstandes

Description of the measurement object

Das Messobjekt ist eine Solarzelle, Typ: PSC/Si. Die Stabilität der Solarzelle wurde nicht untersucht.
The device under test is a PSC/Si solar cell. The temporal stability of the solar cell performance was not controlled.

2. Messverfahren

Measurement procedure

Bestimmt wird der Wert der absoluten differentiellen spektralen Bestrahlungsstärkeempfindlichkeit im Wellenlängenbereich ca. 300-1200 nm bei dem angegebenen Kurzschlussstrom. Die Kalibrierung der Solarzelle wurde mit einem Lasermonochromator mit dem DSR-Messverfahren /1/ und entsprechend /2/ durchgeführt. Die Messung wird im Zweistrahlverfahren durchgeführt und verwendet gleichzeitig:
a) eine stationäre Biasbestrahlung mit Bestrahlungsstärken E_B, welche jedoch nicht explizit gemessen werden. Ihre Variation erlaubt unterschiedliche Kurzschlussströme I_{SC} (E_B), sowie
b) eine zeitlich modulierte, quasi-monochromatische Messstrahlung. Ihre Bestrahlungsstärke wird bestimmt mit einer primarkalibrierten Referenzsolarzelle (rückgeführt: PTB).
The absolute differential spectral responsivity is determined in a wavelength range from 300 nm to 1200 nm at a short circuit current bias.eee The measurement is done with laser-monoochromator setup with the DSR method according to /1/ and /2/ in a two-beam geometry, using the two irradiation beams simultaneously:
a) A stationary bias irradiation with irradiances E_B (not measured explicitly).
The variation of E_B allows different short circuit currents I_{SC} (E_B),
b) A time-modulated quasi-monochromatic measurement irradiation. The irradiance is determined by a primary calibrated reference solar cell (PTB).

Rückführung der Referenzsolarzelle/*Traceability of the reference solar cell* :

Identitäts-Nr. / *Identity-Nr.* :	Kalibrierschein-Nr./ *Certificate-Nr.* :	Rückführung/ *Traceability* :
ISE020059	47033-PTB-21	PTB

3. Messbedingungen

Measurement conditions

Der Arbeitspunkt der Solarzelle wird durch den Bias-Strom im I_{SC} definiert.

The operating point of the solar cell is defined by a bias current under short circuit conditions.

	top cell	bot cell
Bias Strom/*Bias current* :	0.12 mA	0.05 mA
Bias Spannung/Bias voltage:	742.05 mV	644.75 mV
Nominalwert der Temperatur des Messobjekts/ *Nominal Value of the temperature of the object:*	25 °C	25 °C

Die Frequenz des getakteten quasimonochromatischen Messlichtes lag bei 133 Hz. Die spektrale Bandbreite (Halbwertsbreite) liegt unter 5 nm. Die Temperatur der Solarzelle wird mit einem Tastsensor ermittelt und auf (25±0,5)°C eingestellt.

The frequency of the chopped quasi-monochromtatic measurement light is at 133 Hz. The spectral bandwith (full width at half maximum) is below 5 nm. The temperature of the solar cell is determined by a sensor and adjusted to (25±0.5)°C.

CalLab
PV Cells

4. Messergebnis

Measurement results

top cell

Wellenlänge *Wavelength* / nm	*η_{ext} /	*s* / mA*W^{-1}*m²
300.0	0.122	0.00301
310.0	0.152	0.003870
320.0	0.175	0.00458
330.0	0.235	0.00636
340.0	0.291	0.00810
350.0	0.365	0.010482
360.0	0.457	0.0134985
370.0	0.557	0.0168972
380.0	0.650	0.0202320
390.0	0.721	0.0230435
400.0	0.770	0.0252331
410.0	0.796	0.0267498
420.0	0.809	0.0278633
430.0	0.815	0.0287365
440.0	0.817	0.0294758
450.0	0.821	0.0302906
460.0	0.826	0.0311564
470.0	0.835	0.0321516
480.0	0.843	0.0331686
490.0	0.853	0.0342541
500.0	0.863	0.0353823
510.0	0.875	0.0365946
520.0	0.890	0.0379386
528.6	0.902	0.039092
538.7	0.908	0.040100
550.0	0.911	0.0410710
559.0	0.910	0.0416841
567.4	0.907	0.0421776
578.4	0.902	0.0427497
588.3	0.894	0.0431142
597.2	0.887	0.0434015
608.3	0.875	0.0436491
619.1	0.865	0.0438835
628.3	0.857	0.0441542
639.5	0.846	0.0443406
648.0	0.837	0.0444549
661.8	0.822	0.0446066
680.3	0.806	0.0449301
680.3	0.804	0.0448618
690.0	0.797	0.0450610
700.0	0.791	0.0454119
710.0	0.787	0.0457907
720.0	0.773	0.0456087
730.0	0.708	0.0423753

Fraunhofer ISE

CalLab
PV Cells

9005172HMI1020

top cell

Wellenlänge *Wavelength* / nm	*η_{ext} /	*s* / $mA*W^{-1}*m^2$
730.0	0.708	0.0423753
740.0	0.509	0.0308823
750.0	0.228	0.0140204
760.0	0.0701	0.0043702
770.0	0.0185	0.0011671
780.0	0.00552	0.00035310
790.0	0.00149	0.00009677
840.0	0.000389	0.00002680
1020.0	0.000414	0.0000346

Fraunhofer ISE

CalLab PV Cells

9005172HMI1020

bottom cell

Wellenlänge *Wavelength* / nm	*η_{ext} /	*s* / mA*W^{-1}*m²
300.0	0.00153	0.00004
400.0	0.0131	0.00043053
500.0	0.0155	0.00063633
550.0	0.0216	0.0009719
559.2	0.0244	0.0011203
567.4	0.0277	0.0012899
578.4	0.0338	0.0016002
588.3	0.0405	0.0019515
597.4	0.0475	0.0023257
608.3	0.0567	0.0028253
620.9	0.0680	0.0034606
628.3	0.0755	0.00389045
639.7	0.0876	0.0045916
648.0	0.0960	0.0050982
662.4	0.110	0.0059720
680.3	0.126	0.0070013
680.3	0.126	0.0070322
690.0	0.133	0.0075508
700.0	0.139	0.0079843
710.0	0.144	0.00839433
720.0	0.156	0.0092311
730.0	0.215	0.0128486
740.0	0.402	0.0243872
750.0	0.674	0.0414419
760.0	0.832	0.0518295
770.0	0.881	0.0556295
780.0	0.892	0.0570254
790.0	0.898	0.0581562
800.0	0.904	0.0592710
810.0	0.909	0.060358
820.0	0.913	0.061352
830.0	0.916	0.062337
840.0	0.917	0.063169
850.0	0.918	0.0639305
860.0	0.917	0.064617
870.0	0.916	0.065322
880.0	0.916	0.066058
890.0	0.915	0.0667853
900.0	0.915	0.0675261
910.0	0.929	0.069266
920.0	0.925	0.0697639
930.0	0.926	0.070630
940.0	0.929	0.071546
950.0	0.931	0.072477
960.0	0.931	0.0732879
970.0	0.931	0.074017
980.0	0.930	0.074680
990.0	0.927	0.075215

Fraunhofer ISE

CalLab PV Cells

bottom cell

Wellenlänge *Wavelength* / nm	*η_{ext} /	*s* / mA*W^{-1}*m²
990.0	0.927	0.075215
1000.0	0.922	0.075542
1010.0	0.914	0.075632
1020.0	0.900	0.075261
1030.0	0.881	0.074413
1032.0	0.877	0.074228
1032.0	0.878	0.074231
1040.0	0.859	0.073217
1047.8	0.835	0.071717
1068.5	0.745	0.065259
1092.3	0.646	0.057798
1104.9	0.581	0.052593
1115.6	0.517	0.047275
1126.2	0.448	0.041368
1134.0	0.389	0.036188
1142.6	0.326	0.030492
1153.9	0.234	0.02214
1168.4	0.116	0.011145
1171.0	0.0944	0.00907
1171.0	0.0968	0.00930
1179.9	0.0383	0.00370
1194.0	0.0113	0.001108

*Spektrale Bestrahlungsstärkeempfindlichkeit und externe Quanteneffizienz stehen in folgendem Zusammenhang /
Spectral responsivity and External Quantum Efficiency are related as follows:

$$\eta_{\text{ext}}(\lambda) = \frac{J(\lambda)/q}{E(\lambda)/h\nu} = \frac{h\nu}{q}\frac{J(\lambda)}{E(\lambda)} = \frac{hc}{nq\lambda}\frac{s(\lambda)}{a} = 1239{,}8\,\frac{nm \cdot W}{A}\frac{s(\lambda)}{n\lambda a}$$

c: Vakuumlichtgeschwindigkeit/ *speed of light in a vacuum*
h: Planck'sches Wirkungsquantum/ *Planck constant*
q: Elementarladung/ *elementary charge*
n: Brechungsindex Luft/ *refraction index*
$\eta_{ext}(\lambda)$: externe Quanteneffizienz/ *external quantum efficiency*
s(λ): spektrale Bestrahlungsstärkeempfindlichkeit/ *spectral responsivity*
a: Fläche/ *area*

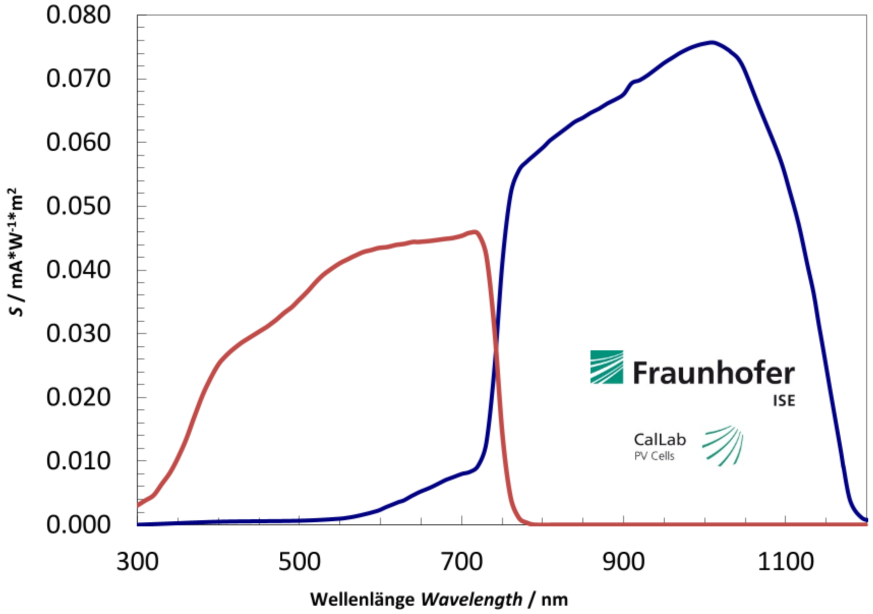

6. Literatur

Literature

/1/ J. Metzdorf, Calibration of Solar Cells. 1: *The Differential Spectral Responsivity Method*, Applied Optics 26 (1987) p.1701-1708

/2/ IEC 60904-8-Ed.3:2014, *Photovoltaic devices - Part 8: Measurement of the spectral responsivity of a photovoltaic (PV) device*

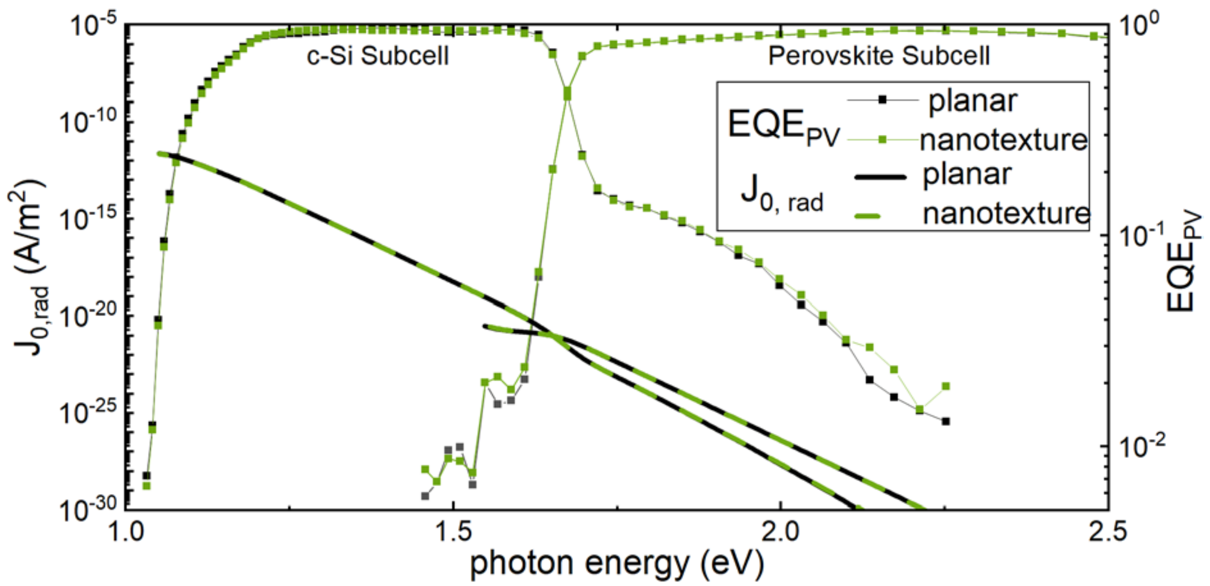

Figure S11 | External quantum efficiency (EQE_{PV}) onset of the silicon and perovskite subcells and their emitted spectral photon flux calculated when the device is in equilibrium with the black-body (BB) radiation of the surroundings at 300K according to equation S1 and S2.

$$J_{0,\mathrm{rad}} = \int \mathrm{EQE}\,\phi_{\mathrm{BB}}\,d\epsilon \qquad \text{(eq. S1)}$$

with

$$\phi_{\mathrm{BB}} = \frac{1}{4\hbar^3 c^2} \cdot \frac{E^2}{\exp\left(\frac{E}{k_B T}\right) - 1} \qquad \text{(eq. S2)}$$

Table S1 | Summary of the derived $J_{0,rad}$ values for the respective perovskite top and silicon bottom cells

	$J_{0,\mathrm{rad}}$ perovskite subcell (A/m^2)	**$J_{0,\mathrm{rad}}$ silicon subcell** (A/m^2)
planar	$3.14\text{x}10^{-21}$	$2.39\text{x}10^{-12}$
nanotexture	$3.42\ \text{x}10^{-21}$	$2.28\ \text{x}10^{-12}$

Table S2 | Details of the 3D optical simulations with the finite element method (FEM)

The materials and layer thicknesses used for the optical simulations presented in Figures 3d-f. All thicknesses (except Si) are given in nm, the bold thicknesses resulted from the Bayesian optimization. The references for refractive index data are given in the second column. Further, the optimized photo-current densities are shown.

		Planar	**Nanotextured**
Lithium fluoride (LiF)	[S1]	110	110
Indium zinc oxide (IZO)	[S2]	90	90
Tin oxide (SnO_2)	[S2]	10	10
C_{60}	[S3]	23	23
Perovskite[1]	[S3]	**563**	**583**[2]
Indium tin oxide (ITO)	[S3]	21	21
Nanocrystalline silicon oxide (nc-SiO_x)	[S4]	**101**	**110**
Intrinsic amorphous hydrogenated Si (a-Si:H)	[S5]	5	5
Crystalline silicon (wafer, Si)	[S6]	300 µm	300 µm
$J_{ph,max}$ (mA/cm^2)		20.22	20.24

1 As we did not have optical data for the perovskite used in this work, we performed the simulations with optical data for the triple-cation perovskite $Cs_{0.05}(MA_{0.17}FA_{0.83})Pb(I_{0.83}Br_{0.17})_3$ with ≈ 1.64 eV bandgap instead. The self-assembled monolayer (SAM) between ITO and perovskite can be omitted in the optical simulations due to its negligible thickness.

2 For the nanotextured device, the perovskite layer is not conformal. The thickness denotes the thickness of a planar layer with the same volume.

Table S3 | Details of the 1D optical simulations with `GenPro4`

The materials and layer thicknesses used for the optical simulations considering the solar cell layer stack shown in Figure 5. All thicknesses (except Si) are given in nm. The references for refractive index data are given in the second column.

		Planar
Lithium fluoride (LiF)	[S1]	110 nm
Indium zinc oxide (IZO)	[S2]	90 nm
Tin oxide (SnO_2)	[S2]	10 nm
C_{60}	[S3]	23 nm
perovskite[1]	[S3]	569 nm
Doped indium oxide (InO) interlayer	[S7]	20 nm
Nanocrystalline silicon oxide (nc-SiO_x)	[S4]	107 nm
Intrinsic amorphous hydrogenated Si (a-Si:H)	[S8]	5 nm
Crystalline silicon (wafer, Si)	[S5]	260 µm
p-doped amorphous hydrogenated Si (p-a:Si:H)	[S4]	10 nm
Doped indium oxide (InO) rear-side	[S7]	10-200 nm 10nm Steps
Silicon oxide (SiO_2)	[S7]	0-300 nm 10 nm Steps
Silver (Ag)	[S9]	400 nm

Table S4 | Quokka3 simulation parameters

Parameter	Value, Property, Model, Variation	Unit
Dimensions	2	
Unit Cell Thickness	260	μm
Unit Cell width	20000	μm
_		
Material Group		
Optical Generation Model Type	Text-Z model obtained from GenPro4 Simulation	
Auger Model	Si-Altermatt2011	
Radiative Recombination Model	Si-Nguyen	
Density of State	Si-Green1990	
Intrinsic Carrier Density Model	user-const	
Intrinsic Carier Density n_{i0}	9.65e9	cm^{-3}
Silicon Mobiylity Model	Si-Klaassen1992	
Si Band Gap Narrowing Model	Si-Schenk1998	
Doping Setting Type	dopingtype-resistivity	
Doping Type	n-type	
Doping Resistivity	3	Ωcm
Bulk Recombination Type	intrinsic plus SRH	
Bulk Recombination SRH Type	τ-E_t	
Bulk Recombination SRH τ_n	1000	μs
Bulk Recombination SRH τ_p	10000	μs
Bulk Recombination SRH τ E_t-E_i	0	eV
Electron Selective Contact		
Geometry Plane	front	
Geometry Shape	full	
Electrical Model Type	lumped	
Sheet Resistance (R_{sh})	0.001	Ω
Conduction Type	n-type	
Vertical Resistivity Type	ohmic	
Vertical Resistivity	0.05	Ωcm^2
Contact Recombination Type	Surface effective Recombination (S_{eff})	
Contact Recombination S_{eff}	1.2	cm/s
Electron Contact Feature		
Geometry Plane	front	
Geometry Shape	full	
Ohmic Resistivity (TCO/Metal)	3e-4	Ωcm^2
Current Transport Model	ohmic	
_		
Electron Metal Feature		
Geometry Plane	front	
Geometry Shape	full	
Polarity	n-type	
Sheet Resistance (R_{sh})	1.5e-3	Ω
Shading Fraction	0	
_ **Hole Selective Contact**		

Geometry Plane	rear	
Geometry Shape	full	
Electrical Model Type	lumped	
Sheet Resistance (R_{sh})	95-216	Ω
Conduction Type	p-type	
Vertical Resistivity Type	ohmic	
Vertical Resistivity	0.2	Ωcm²
Contact Recombination Type	Surface effective Recombination (S_{eff})	
Contact Recombination S_{eff}	1.2	cm/s
Hole Contact Feature		
Geometry Plane	rear	
Geometry Shape	rectangle	
Geometry Size X (width)	40	μm
Geometry Pitch X (finger pitch)	500-2500	μm
Ohmic Resistivity (TCO/Metal)	1e-5	Ωcm²
Current Transport Model	ohmic	
Hole Metal Feature		
Geometry Plane	rear	
Geometry Shape	rectangle	
Geometry Size X (width)	40	μm
Geometry Pitch X (finger pitch)	500-2500	μm
Polarity	p-type	
Sheet Resistance (R_{sh})	1.5e-3	Ω
Shading Fraction	0	

[S1] H. H. Li, ''Refractive index of alkali halides and its wavelength and temperature derivatives,'' J. Phys. Chem. Ref. Data, vol. 5, no. 2, pp. 329–528, 1976. doi.org/10.1063/1.555536

[S2] M. Jošt, E. Köhnen, A. B. Morales-Vilches, et al., ''Textured interfaces in monolithic perovskite/silicon tandemsolar cells: advanced light management for improved efficiency and energy yield,'' Energy Environ. Sci., vol. 11, no. 12, pp. 3511–3523, 2018. doi.org/10.1039/C8EE02469C

[S3] A. Tejada Esteves, Personal Communication. 2020

[S4] L. Mazzarella, M. Werth, K. Jäger, et al., ''Infrared photocurrent management in monolithic perovskite/silicon heterojunction tandem solar cells by using a nanocrystalline silicon oxide interlayer,'' Optic Express, vol. 26, no. 10, p. A487, 2018. Doi.org/10.1364/OE.26.00A487

[S5] K. Jäger, L. Korte, B. Rech, and S. Albrecht, "Numerical optical optimization of monolithic planar perovskite-silicon tandem solar cells with regular and inverted device architectures". *Opt. Express* 25, A473 (2017).

[S6] M. A. Green and M. J. Keevers, ''Optical properties of intrinsic silicon at 300 K,'' Prog. Photovoltaics Res. Appl., vol. 3, no. 3, pp. 189–192, 1995. doi.org/10.1002/pip.4670030303

[S7] Cruz, A. *et al.* Optoelectrical analysis of TCO$\mathplus$Silicon oxide double layers at the front and rear side of silicon heterojunction solar cells. *Solar Energy Materials and Solar Cells* 236, 111493 (2022).

[S8] Chen, B. et al. Blade-Coated Perovskites on Textured Silicon for 26%-Efficient Monolithic Perovskite/Silicon Tandem Solar Cells. Joule 4, 850–864 (2020).

[S9] Yajie Jiang, Supriya Pillai and Martin A. Green, 'Realistic Silver Optical Constants for Plasmonics', Scientific Reports**, vol. 6, no.** 1, pp.30605, (2016)